Unexpected space weather causing the reentry of 38 Starlink satellites in February 2022

Ryuho Kataoka (1,2,3), Daikou Shiota (4), Hitoshi Fujiwara (5), Hidekatsu Jin (4), Chihiro Tao (4), Hiroyuki Shinagawa (4), and Yasunobu Miyoshi (6)

(1) National Institute of Polar Research
(2) The Graduate University for Advanced Studies, SOKENDAI
(3) Okinawa Institute of Science and Technology
(4) National Institute of Information and Communications Technology
(5) Faculty of Science and Technology, Seikei University
(6) Department of Earth and Planetary Sciences, Faculty of Science, Kyushu University

Abstract

The accidental reentry of 38 Starlink satellites occurred in early February, 2022, associated with the occurrence of moderate magnetic storms. Poorly understood structure of coronal mass ejections (CMEs) caused the magnetic storms at unexpected timing. Better understanding of minor CME structures is therefore necessary for modern space weather forecast. The "up to 50%" enhancement of air drag force was observed at ~200 km altitude, preventing the satellites from their safety operations. Although the mass density enhancement predicted by the NRLMSIS2.0 empirical model is less than 25 % under the present moderate magnetic storms, the real-time GAIA simulation showed the mass density enhancement of up to 50%. Further, the GAIA simulation suggests that the actual thermospheric disturbances at 200 km altitude may occur with larger amplitude in the wider area than previously thought.

This manuscript has been submitted for publication in Journal of Space Weather and Space Climate. Please note that, despite having undergone peer-review, the manuscript has yet to be formally accepted for publication. Subsequent versions of this manuscript may have slightly different content. If accepted, the final version of this manuscript will be available via a link on this webpage.

1. Introduction

Satellite drag is sensitive to the space weather and space climate, and the social impact is high in the modern society depending on thousands of satellites. There have been unfortunate accidents of satellite reentry due to the enhanced drag during large magnetic storms, including the old example of the Bastille event in July 2000 when the Japanese ASKA satellite orbiting at 440 km was attitude-disturbed, lost the solar power, and finally reentered. The most recent example of Starlink satellites was rather surprising (Hapgood et al., 2022) because of the large number of lost satellites (38 out of 49) at one time associated with the occurrence of moderate magnetic storms.

SpaceX launched the 49 Starlink satellites at 1813 UT on February 3. From the initial perigee of 210 km, the satellites were planned to raise the altitude up to ~340 km in the Low-Earth Orbit (LEO). This was a challenging attempt for SpaceX, targeting relatively low altitude where the atmospheric drag is critical, partly to obtain the data for controlling space debris for future. In the press release on February 8 (https://www.spacex.com/updates/, February 8, 2022: GEOMAGNETIC STORM AND RECENTLY DEPLOYED STARLINK SATELLITES), SpaceX noted the space weather situation and operation as follows "*... onboard GPS suggests the escalation speed and severity of the storm caused atmospheric drag to increase up to 50 percent higher than during previous launches. The Starlink team commanded the satellites into a safe-mode where they would fly edge-on (like a sheet of paper) to minimize drag to effectively "take cover from the storm" and continued to work...*"

In general, geomagnetic disturbances (GMD) result in the Joule heating in the polar atmosphere, and therefore enhance the mass density in the expanding thermosphere. The drag force of spacecraft is proportional to the mass density of the thermosphere. Therefore, unless we succeed to predict the GMD, we cannot predict the satellite drag.

In order to investigate the themospheric mass density variations, we consult the real-time results (Tao et al., 2020) of the Ground-to-topside model of Atmosphere and Ionosphere for Aeronomy (GAIA) (e.g., Jin et al., 2011). Several kinds of thermospheric disturbances caused by the lower atmospheric and magnetospheric phenomena have been successfully reproduced by GAIA (Miyoshi et al., 2012; Jin et al., 2012; Shinagawa et al., 2017; Miyoshi et al., 2018).

The purpose of this paper is to examine our capability of space weather forecast for this particular GMD event, especially focusing on the puzzling parts for space weather forecasters and satellite operators. We hope this work contributes to accumulate our knowledge for future robust satellite operations.

2. Solar eruptions

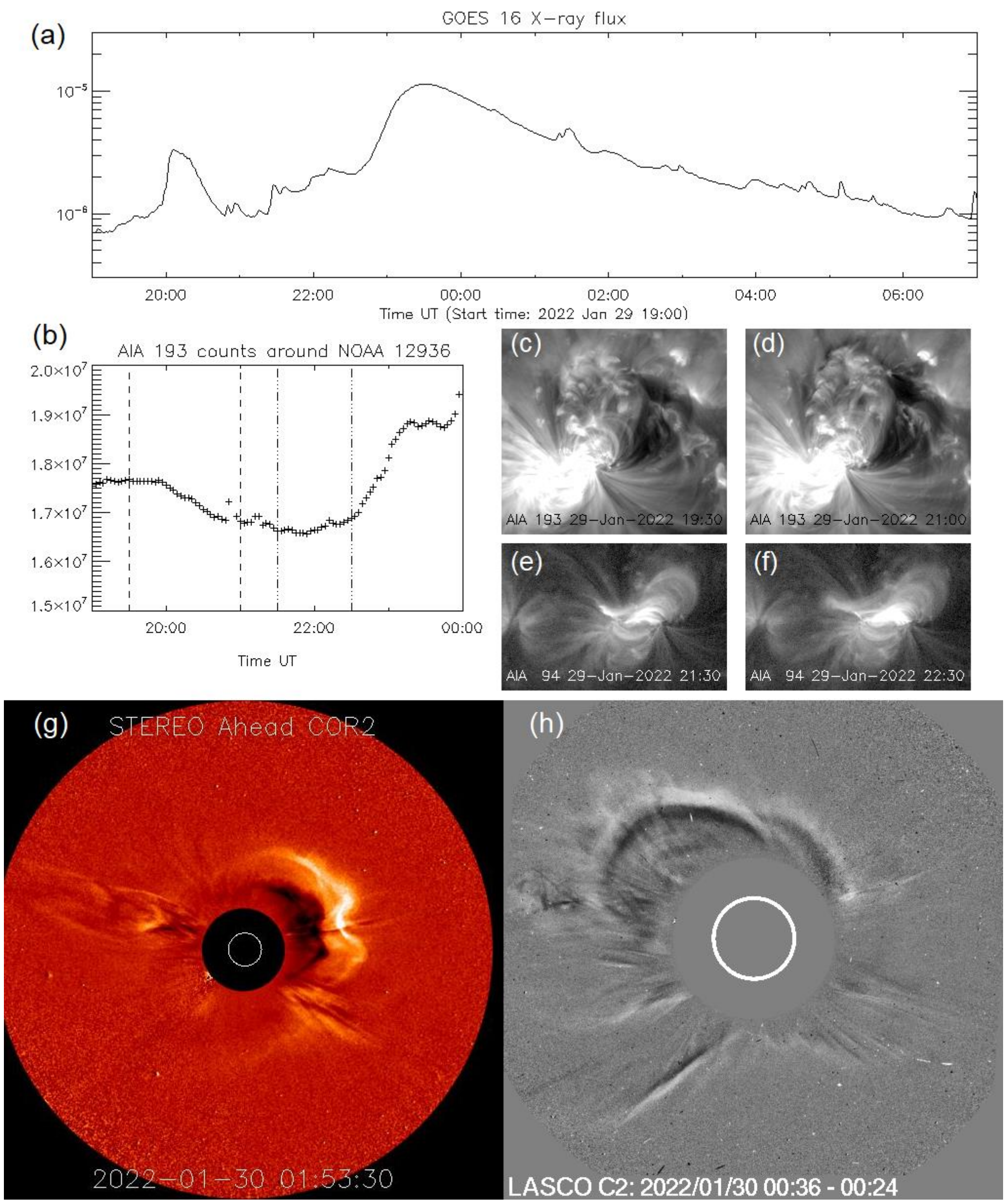

Figure 1. Solar flare, coronal dimming, and eruptions. Data used are from GOES 16 X-ray flux, SDO/AIA 193 and 94, STEREO-A/ COR2, and SOHO/LASCO.

M1.1 class solar flare occurred at 2332 UT on Jan. 29, 2022 (**Figure 1a**), in the active region (AR) NOAA12936 located near the central meridian of the solar disc. Before the flare peak, a coronal dimming was observed by SDO/AIA at ~2000 UT (**Figure 1b**) near the northern envelope of the AR together with several brightenings in the central region (**Figures 1c and 1d**). Around 2200 UT a coronal loop in the central region expanded outward and eastward and the M1.1-class long duration event (LDE) flare occurred (**Figures 1e and 1f**).

Associated with the LDE flare, a halo CME was observed at 23:48 UT in SOHO/LASCO images and at 23:53UT in STEREO-A/SECCHI COR2 images. The apparent propagation speeds of the CME in images of LASCO and COR2 were approximately 620 km/s and 440 km/s, respectively. The simply expected arrival time to 1 AU distance is therefore ranging from early February 2 to the end of February 2. Note that STEREO-A was located at ~35 deg longitude behind the Earth. The CME edge is toward north-east at LASCO, while it looks rather isotropic at COR2, which is consistent with the observed early CME arrival at STEREO-A. It is possible that two CMEs appeared overlapped in **Figure 1h**, one can be associated with the coronal dimming and another can be associated with LDE flare. Although the "post-mortem" analysis can identify such a possibility, it was difficult for forecasters to utilize the information of possibly double CMEs for actual GMD forecast, as described in the following Sections.

3. Geomagnetic disturbances

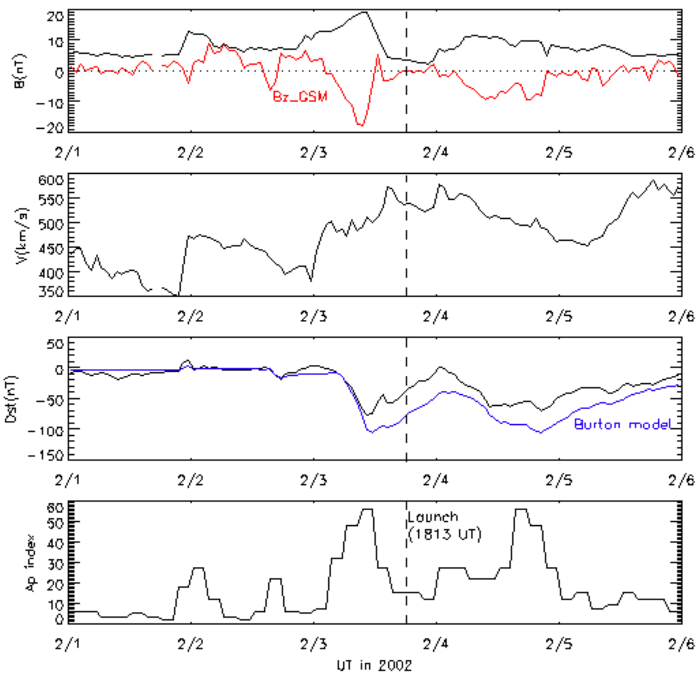

Figure 2. OMNI-2 hourly data. Magnetic field strength (red curve is Bz in GSM coordinate system), solar wind speed, Dst index (blue curve shows the result from Burton model), and Ap index.

As shown in **Figure 2**, magnetic storms peaked at 1100 UT on February 3 (Dst = -77 nT) and 1100 UT on February 4 (Dst = -64 nT). The W-shape variation in the Dst index is characterized by the positive excursion in the middle of moderate storms at 0000 UT on February 4 (Dst peak = 4 nT). Note that the whole W-shape pattern took ~2 days, which is essentially different from the typical two-step development of magnetic storms taking less than 1 day (Kamide et al., 1998).

Looking back the Dst record for the last 20 years, for example, similar W-shape Dst variation can be identified on July 9-10, 2005 and on March 24-25, 2007. The July 2005 GMD event is caused by the arrival of CME just after a moderate storm, while March 2007 GMD event is caused by the arrival of corotating interaction region (CIR) after a CME storm. Therefore, these former examples are understandable by the standard pictures of CME storms and CIR storms (Kataoka and Miyoshi, 2006), and the second Dst peak is easily expected for any forecasters in advance by the arrivals of shock and stream interface, respectively.

However, the February 2022 GMD event is different from such a standard picture with respect to the following two points. First, the leading edge of the first flux rope arrived ~1 day later from the shock arrival at 2220 UT on February 1. Here many experts expected at that time that the oncoming flux rope did not likely hit the Earth anymore because the sheath duration is much longer than the standard value of 6-12 hours. After all, the first storm was driven by the very late arrival of the first flux rope on February 3. Another puzzling feature then came next at the end of the first storm, when the Earth exited the first flux rope. It seemed a reasonable (moderate and settling GMD) timing for the launch of Starlink satellites indeed (1813 UT on February 3). Then, surprisingly, the second flux rope arrived just after the full recovery of the first storm, and the main phase of the second storm readily started on February 4, which must have confused the initial satellite operations. These two major concerns documented above can be addressed in more detail and better clarified by combining another in-situ solar wind observation data at STEREO-A at different longitude (~35 deg behind in longitude from the Earth), as shown in Section 4.

If we knew the arrival of two flux ropes in advance, the expectation and even rough prediction of these two moderate storms itself was not likely a difficult task. For example, the simplest Burton model (Burton et al., 1975; O'Brien and McPherron, 2000) roughly works to predict the Dst variation (Figure 2, blue curve). Further, if we knew the occurrence of these moderate storms, the thermospheric response (mass density enhancement at desired altitude) can also be roughly predictable by empirical model such as NRLMSIS2.0, as a function of ap index. The more detailed dynamic response can be clarified by real-time GAIA simulation, as discussed in Section 5.

4. Interplanetary structure of coronal mass ejections

The different look of the overall shock-CME passage at different longitude can be recognized by comparing the in-situ observation of interplanetary magnetic field (IMF), as shown in **Figures 3 and 4**. It is interesting to note that the STEREO-A data looks like a standard picture of shock-CME passage (Kataoka and Miyoshi, 2006), which was natural especially at the head-on location against the propagating CME. However, at the Earth position, as shown in **Figure 4**, the overall structure looks elongated, and nearly doubled in time or space, which clearly indicated the flank-side passage of CME.

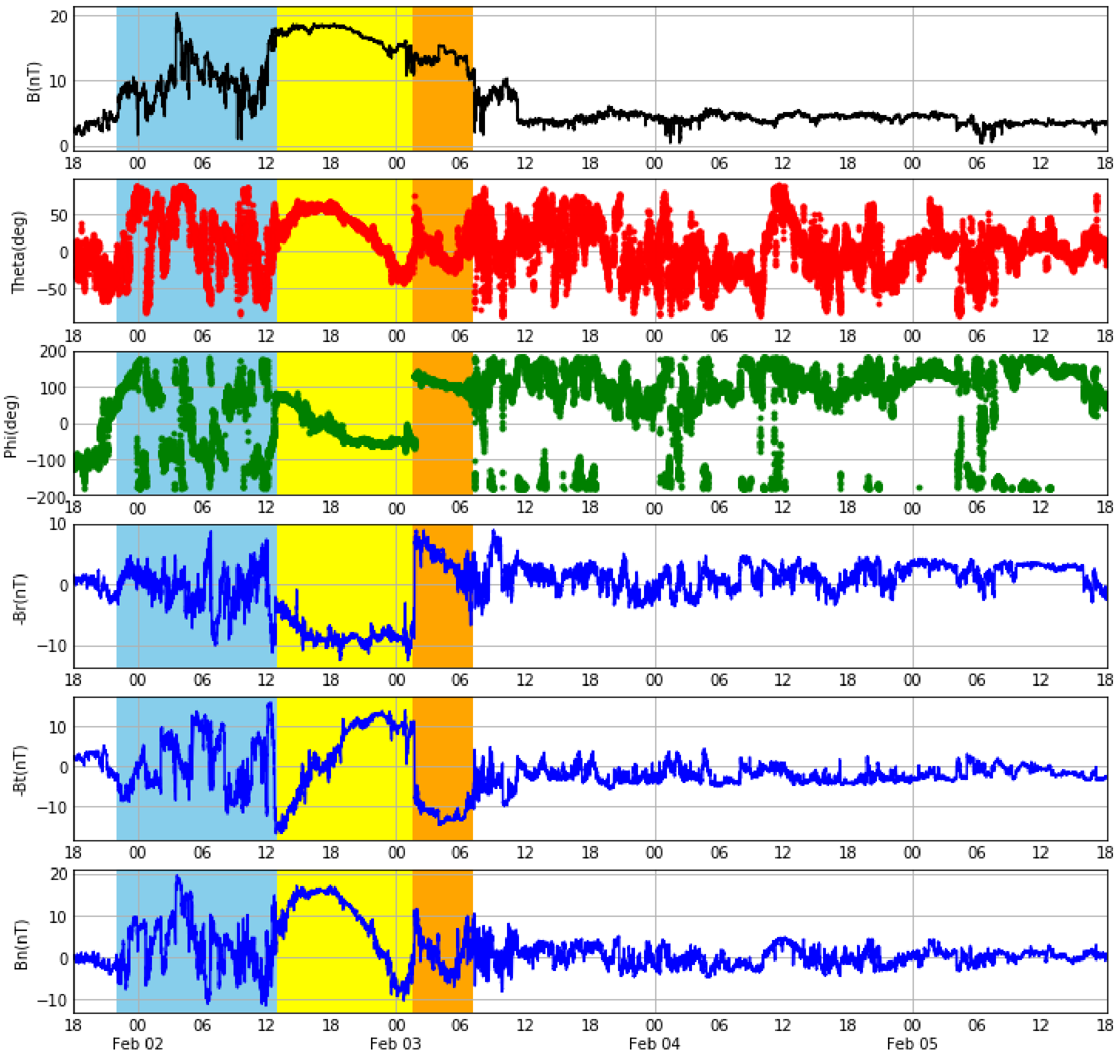

Figure 3. STEREO-A/IMPACT data. From top to bottom, magnetic field strength, latitude (theta), azimuth angle (phi), Bx (negative BR), By (negative BT), and Bz (=BN).

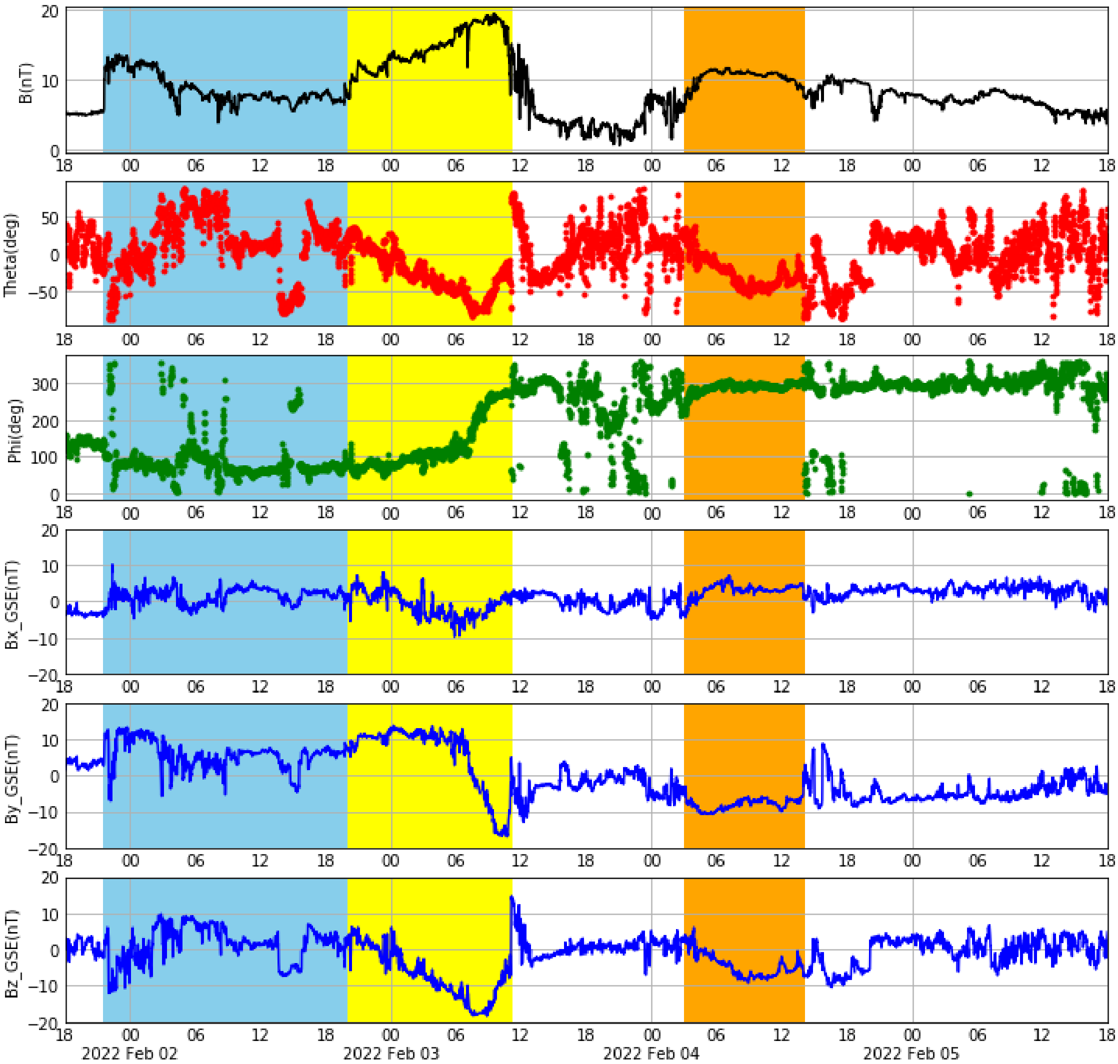

Figure 4. DSCOVR magnetic field data. From top to bottom, magnetic field strength, latitude (theta), azimuth angle (phi), Bx, By, and Bz in GSE coordinate system.

Similarities exist in the first flux rope. The West-North-East (and to South) rotation at STEREO-A and North-East-South (and to West) rotation at DSCOVR are in the same helicity sense, just tilted by ~90 deg. Such a relationship of ~90 deg tilt of the flux rope is also consistent with the rough picture of head-on and flank-side passages of the same flux rope. For the second flux rope identified in DSCOVR data, similar trailing part of the CME (orange shaded, small B field rotation merging to Parker spiral) can be identified in STEREO-A data (**Figure 3**).

The outstanding difference is the weak-B region (continued for more than half day from 1200 UT on February 3) in DSCOVR data, which separated the two flux ropes. The appearance of the weak-B region is far from the standard picture, and it would be impossible for forecasters to expect the very late arrival of the second flux rope at the Earth.

There are at least two possibilities to cause the weak-B region. The large-scale IMF direction changed from away to toward before and after the CME, and the heliospheric current sheet (HCS) must be located somewhere around the weak-B region. The weak-B region can therefore be a product of the interaction between the CME flux rope and the HCS, which should be complex enough to be different at different longitude. Another interpretation is that there were originally two flux ropes, as indicated in **Figure 1**, and illustrated in **Figure 5**, which appeared sticked together at the STEREO-A position but appeared separated at the Earth. The detailed modeling to examine several possibilities is beyond the scope of this paper, although it would provide a good challenging material for future advanced modeling work.

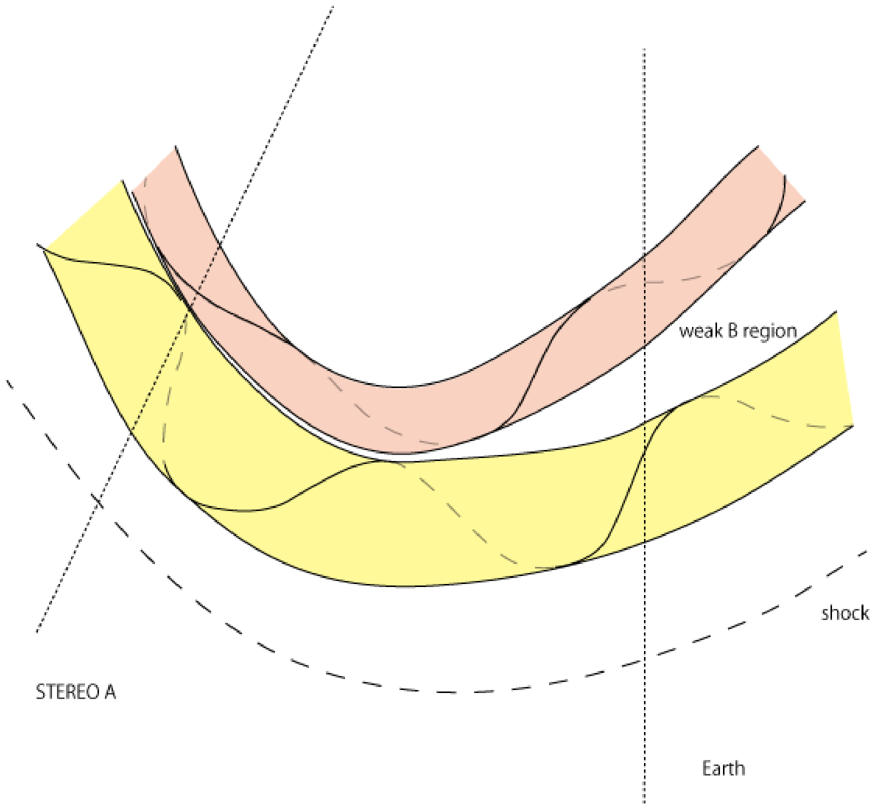

Figure 5. Schematic illustration of two flux ropes encountering the DISCOVR (Earth) and STEREO-A spacecraft at ~1 AU.

5. Thermospheric response to the geomagnetic disturbance

The thermospheric variations during the moderate storm periods were simulated using real-time GAIA with the empirical high-latitude electric potential model presented by Weimer (1995). The solar wind data obtained by DSCOVR were used for the Weimer model. **Figure 6** shows the global distributions of the thermospheric mass density at quiet (0000 UT on February 4, 2022) and disturbed (2100 UT on February 4, 2022) periods.

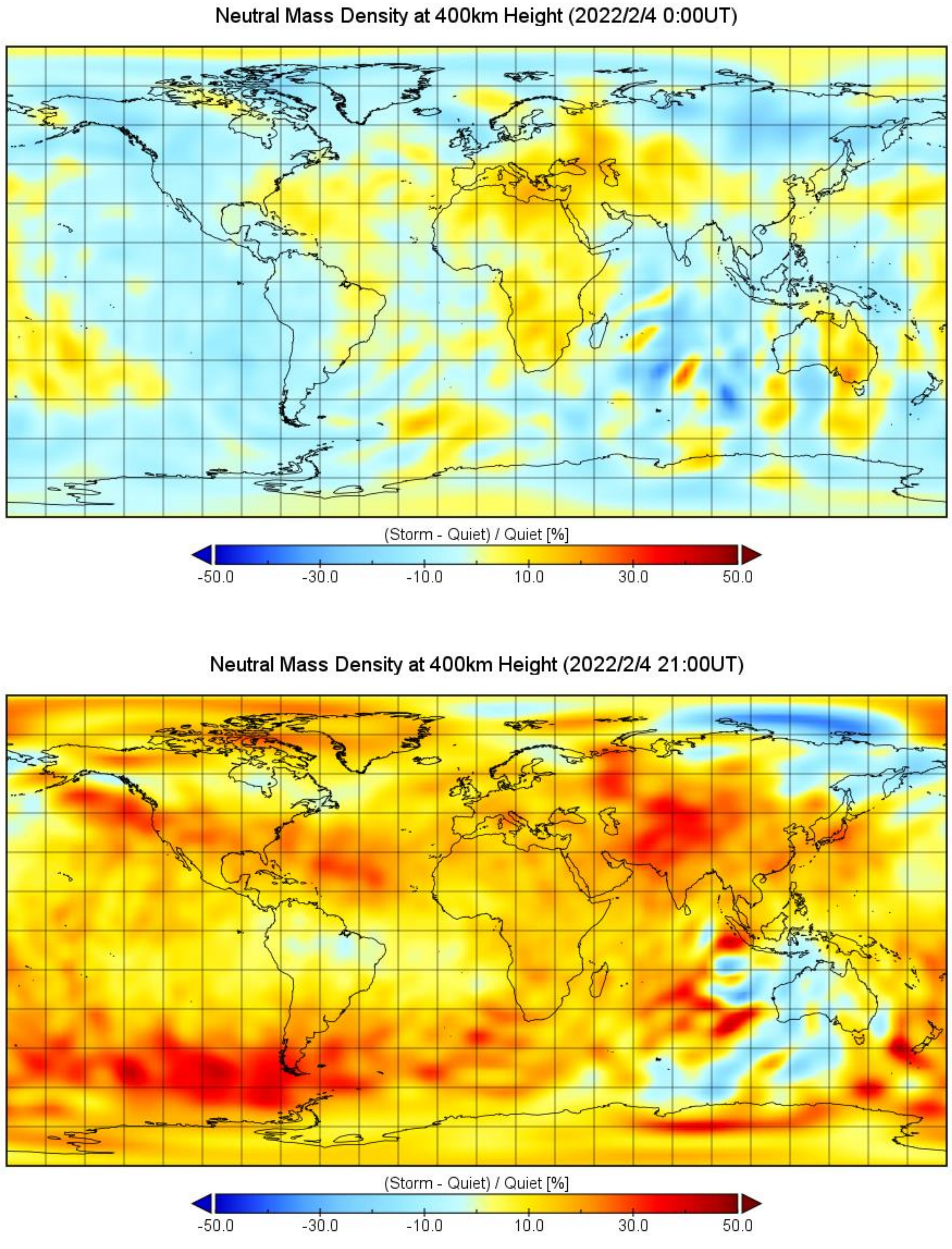

Figure 6. Simulation results of the thermospheric mass density at 400 km altitude, (storm-quiet)/quiet

in %, for 0000 UT and 2100 UT on February 4, 2022. The selected quiet day is February 1, 2022.

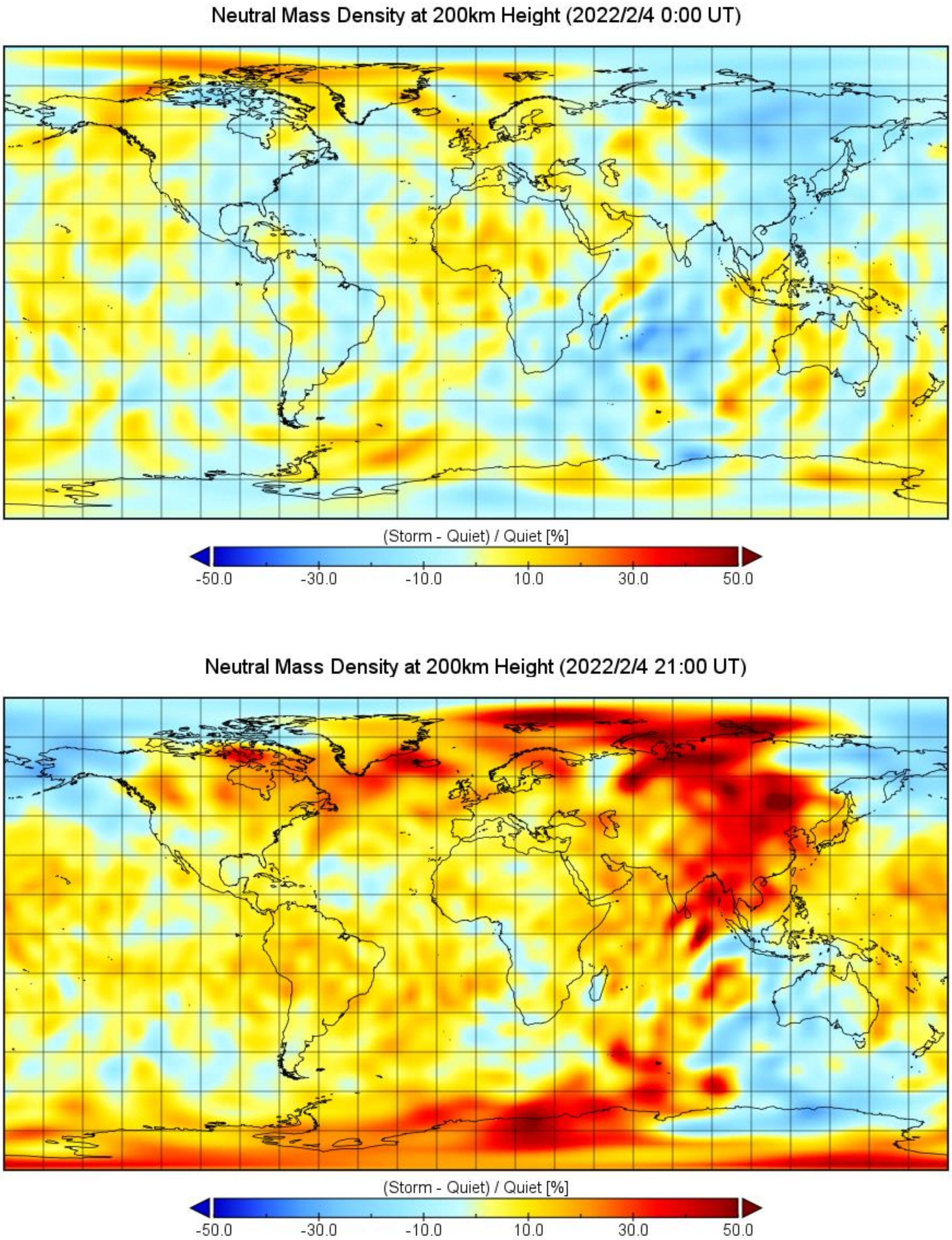

Figure 7. Simulation results of the thermospheric mass density at 200 km altitude, (storm-quiet)/quiet in %, for 0000 UT and 2100 UT on February 4, 2022. The selected quiet day is February 1, 2022.

The simulation results in **Figures 6 and 7** show significant enhancements of the thermosheric mass density (up to 50 % at both the 200 and 400 km altitudes) in the wide area before and after the second magnetic storm. The up to 50 % enhancements of the thermospheric mass density indicate the enhancements of the drag force to the satellites passing through these altitude regions, which is consistent with the documentation of SpaceX.

In fact, the 50% drag increase was not higher than expected. For example, at 200 km altitude, ~25 % increase by enhanced geomagnetic activity can be expected from the empirical model, NRLMSIS2.0 (Emmert et al., 2020), as shown by **Supplemental Information Movie A1-A4**. Also, the actual density variation can be largely deviated from the empirical model, such as so-called "cellular structure" (Crowley et al., 1996), which can easily explain the additional 25% variation. Comparing with the previous studies, the present simulation seems to show the thermospheric mass density enhancements in wider area.

In addition, the GAIA simulation results suggest that the wave-like patterns are superimposed on the mass density enhancements, which was likely caused by horizontal expansion of the heated air (**Supplemental Information Movies B1-B4**). Therefore, the actual thermospheric disturbances at around 200 km altitude might occur with larger amplitude in the wider area than those we thought in some cases. It is therefore important to improve our understanding of the theremosphere, by examining the accuracy and limitation of the simulation results, comparing with the actual in-situ observations.

6. Summary and conclusions

We showed that the occurrence of moderate storms at unexpected timings on February 3-4, 2022 caused the accidental reentry of 38 Starlink satellites. The important lessons learned from this GMD event are: 1) In real-time, it was difficult to expect the arrivals of two separated flux ropes from the possible overlapped appearance of CMEs. 2) It was also difficult to accurately predict the solar wind profiles by the flank-side passage of CMEs. 3) Further, the real-time simulation of the thermosphere was necessary to nowcast the 50% mass density enhancement. We are entering the new age, to quantitatively address the hard-to-predict and poorly-understood minor CME structures, by utilizing multi-spacecraft observations in the upstream solar wind, combined with realistic CME and solar wind simulations. For future satellite operation safety, we would also need better understanding of the possible errors and limitation of cutting-edge simulations of the thermosphere.

Acknowledgments:

We would like to thank the use of real-time open data from SDO, SOHO, STEREO-A, DSCOVR. The

Dst and ap indices are provided from Kyoto University, via NASA/OMNI website. RK thanks Okinawa Institute of Science and Technology for hosting his sabbatical visit. DS is supported by JSPS KAKENHI 21H04492. YM, HJ, CT, HS, HF are supported by JSPS KAKENHI 21H01150, JP20K04037. HJ and HS are supported by 20K04037.

References:

Burton, R. K., McPherron, R. L., and Russell, C. T. (1975), An empirical relationship between interplanetary conditions and Dst, J. Geophys. Res., 80(31), 4204-4214, doi:10.1029/JA080i031p04204.

Crowley, G., Schoendorf, J., Roble, R. G., and Marcos, F. A. (1996), Cellular structures in the high-latitude thermosphere, J. Geophys. Res., 101(A1), 211-223, doi:10.1029/95JA02584.

Emmert, J. T., Drob, D. P., Picone, J. M., Siskind, D. E., Jones, M. Jr., Mlynczak, M. G., et al. (2020). NRLMSIS 2.0: A whole‐atmosphere empirical model of temperature and neutral species densities. Earth and Space Science, 7, e2020EA001321. https://doi.org/10.1029/2020EA001321.

Jin, H., Y. Miyoshi, H. Fujiwara, H. Shinagawa, K. Terada, N. Terada, M. Ishii, Y. Otsuka, and A. Saito (2011), Vertical Connection from the Tropospheric Activities to the Ionospheric Longitudinal Structure Simulated by a New Earth's Whole Atmosphere-Ionosphere Coupled Model, J. Geophys. Res., 116, A01316, doi:10.1029/2010JA015925.

Jin, H., Y. Miyoshi, D. Pancheva, P. Mukhtarov, H. Fujiwara, and H. Shinagawa (2012), Response of migrating tides to the stratospheric sudden warming in 2009 and their effects on the ionosphere studied by a whole atmosphere-ionosphere model GAIA with COSMIC and TIMED/SABER observations, J. Geophys. Res., 117, A10323, doi:10.1029/2012JA017650.

Hapgood, M., Liu, H., & Lugaz, N. (2022). SpaceX-Sailing close to the space weather? Space Weather, 20, e2022SW003074. https://doi.org/10.1029/2022SW003074.

Kamide, Y., N. Yokoyama, W. Gonzalez, B. T. Tsurutani, I. A. Daglis, A. Brekke, and S. Masuda (1998), Two-step development of geomagnetic storms, J. Geophys. Res., 103, A4, 6917-6921.

Kataoka, R., and Y. Miyoshi (2006), Flux enhancement of radiation belt electrons during geomagnetic storms driven by coronal mass ejections and corotating interaction regions, Space Weather, 4, S09004, doi:10.1029/2005SW000211.

Miyoshi, Y., H. Jin, H. Fujiwara, H. Shinagawa and H. Liu (2012), Wave-4 structure of the neutral density in the thermosphere and its relation to atmospheric tide, J. Sol.-Terr. Phys., 90-91, 45-51, https://doi.org/10.1016/j.jastp.2011.12.002.

Miyoshi Y., Jin, H., Fujiwara, H., and H. Shinagawa (2018), Numerical Study of Traveling Ionospheric Disturbances Generated by an Upward Propagating Gravity Wave, J. Geophys. Res.: Space Physics, 123, 2141-2155, doi:10.1002/2017ja025110.

O'Brien, T. P., and McPherron, R. L. (2000), An empirical phase space analysis of ring current dynamics: Solar wind control of injection and decay, J. Geophys. Res., 105(A4), 7707-7719, doi:10.1029/1998JA000437.

Shinagawa, H., Y. Miyoshi, H. Jin, and H. Fujiwara (2017), Global distribution of neutral wind shear associated with sporadic E layers derived from GAIA, J. Geophys. Res. Space Physics, 122, doi:10.1002/2016JA023778.

Tao, C., Jin, H., Miyoshi, Y., Shinagawa, H., Fujiwara, H., Nishioka, M., and Ishii, M. (2020), Numerical forecast of the upper atmosphere and ionosphere using GAIA. Earth Planets Space 72, 178. https://doi.org/10.1186/s40623-020-01307-x.

Weimer, D. R. (1995), Models of high-latitude electric potentials derived with a least error fit of spherical harmonic coefficients, J. Geophys. Res., 100(A10), 19595-19607, doi:10.1029/95JA01755.

Supplemental Information:

Movies A1-A4: Results from NRLMSIS2.0 model. The selected altitudes are 200 km and 400 km, and selected days are Feb. 3 and 4. Observed ap index was used every three hours.

Movies B1-B4: Results from real-time GAIA simulation. The selected altitudes are 200 km and 400 km, and selected days are Feb. 3 and 4.